

A Validation and Uncertainty Quantification Framework for Eulerian-Eulerian Two-Fluid-Model based Multiphase-CFD Solver.

Part II: Applications

Yang Liu^{1,*}, Nam Dinh¹, Ralph Smith²

1 Department of Nuclear Engineering, North Carolina State University, Raleigh, NC 27606, USA

2 Department of Mathematics, North Carolina State University, Raleigh, NC 27607, USA

Abstract

This paper is the second part of a two-part series, which introduces and demonstrates a Validation and Uncertainty Quantification (VUQ) framework that serves two major purposes: i). quantify the uncertainties of the closure relation parameters and predictions of the Multiphase Computational Fluid Dynamics (MCFD) solver; ii). evaluate the agreement between the solver predictions and the experimental measurements. The framework, with the corresponding theory and method, are outlined in the first part paper. In this paper, the workflow of the framework is implemented and demonstrated for two relevant case studies: the wall boiling heat transfer in subcooled boiling flow and the adiabatic bubbly flow. The influential closure relation parameters for multiple quantities of interest (QoIs) are identified through two different global sensitivity analysis (GSA) methods: Morris screening and Sobol indices. The model form uncertainty and model parameter uncertainty of relevant closure relations are evaluated using the “modular Bayesian” approach. The uncertainties of QoIs are quantified by propagating the obtained uncertainties through the solver. The agreement between solver predicted QoIs and the experimental measurement are evaluated using two different validation metrics: confidence interval and area metric. The results demonstrate the applicability of the framework.

1. Introduction

The predictive capability of a MCFD solver depends on answering one question: is this solver adequately representing the underlying physics of a multiphase system of interest? A way to answer this question is to perform the validation and uncertainty quantification (VUQ) for the solver. In the first part of this two-part paper, a VUQ framework is proposed, which consists of a general procedure with six steps. The framework answers the question with two outcomes: i). the uncertainties of the closure relation parameters and predictions of the MCFD solver; ii). the agreement between the solver predictions and the experimental measurements. In this paper, the proposed framework is tested for two case studies of different two-phase flow scenarios.

* Corresponding author.

Email address: yliu73@ncsu.edu (Y.Liu), ntinh@ncsu.edu (N.Dinh), rsmith@ncsu.edu (R.Smith)

There are multiple quantities of interest (QoIs) for a multiphase flow related problem. For example, in a typical boiling system, nucleate boiling in the heated surface evolves from partial to fully-developed and eventually reaches a boiling crisis. Accurately predicting this heat transfer process is vital for the efficiency and safety analysis of a two-phase flow and boiling system. Thus the wall superheat and wall heat transfer are considered as QoIs for boiling related problems. Also, the flow dynamics of the two-phase system is of vital importance for industrial applications. In a nuclear reactor, the void fraction distribution in the BWR fuel assembly significantly influences the reactivity of the core. Moreover, in a steam generator tube, the bubbly dynamics is considered to be a major influence factor to the flow induced vibration, which is a threat to the structure integrity (Pointer and Liu,2017). Thus, the distribution of void fraction and bubble velocity are also considered as QoIs for the two phase flow related problems.

Strictly speaking, a complete VUQ for a MCFD solver requires taking all the QoIs from a scenario into consideration, quantifying the uncertainties of the solver predictions of all those QoIs and corresponding closure relation parameters, then evaluating the agreement between the solver predictions and the experimental measurement. This is compatible with the total data-model integration (TDMI) approach whose fundamental idea is to take all the available experimental data, the relevant closure relations, and the solver into simultaneous consideration for the VUQ process. The TDMI approach serves as the basic idea of this proposed VUQ framework and is achieved with the Bayesian method. Thus such VUQ requirement is compatible with the framework. On the other hand, the complete VUQ requires the support of the measurements for all the QoIs in a given scenario. This includes measurements of the phasic velocities, the void fraction, the pressure drop, the temperature, and the wall heat transfer, etc. It is impractical to measure all the phenomena in a single experimental facility. Moreover, the lack of a satisfactory scaling method for two phase flow system prohibits the use of experimental data from different facilities into one complete VUQ process of the MCFD solver.

In this paper, the limitation of available experimental data is considered, and a more practical approach for the VUQ of the MCFD solver is applied. The VUQ of MCFD is decomposed into two separate case studies. One focuses on the wall heat transfer in the scenario of subcooled flow boiling in a vertical channel, the other focuses on the flow dynamics in the scenario of adiabatic bubbly flow. The decomposition is depicted in Figure 1.

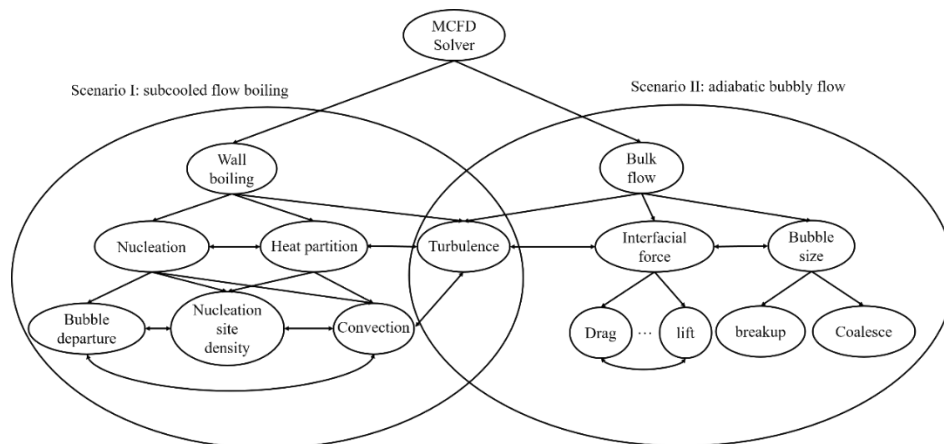


Figure 1. Decomposition of VUQ case studies

As discussed in the first paper, the proposed VUQ framework has a six-step workflow procedure. In this paper, two cases studies are discussed following this procedure. An MCFD solver developed based on open source CFD toolbox OpenFOAM (Weller et al., 1998) is evaluated in the following work, the UQLab package (Marelli and Sudret,2014) is used for sensitivity analysis.

2. Case study I: VUQ on wall boiling heat transfer

2.1 Solver evaluation and data collection

The scenario investigated in this case study is the subcooled flow boiling, with a focus on the wall heat transfer behavior. In this case study, the wall superheat and the three heat transfer components, i.e. evaporation heat transfer, quenching heat transfer, and forced convective heat transfer, are chosen to be the QoIs.

Although the boiling process is crucial for a two phase flow system, the traditional experiments can only measure the wall superheat through thermocouples, as in (Bartolomei and Chanturiya,1967). Hence the previous validation efforts for the boiling related scenario can only be performed for the wall superheat (Krepper et al., 2007).

Recently, the experiments using IR camera makes it possible to measure the detailed wall temperature development in boiling process, thus making the derivation of wall heat transfer components possible (Jung and Kim,2014), (Y. Liu and Dinh,2016), (Yoo et al., 2016), (Bucci et al., 2016).

In this work, the experimental data is collected from (Richenderfer et al., 2017), which measures the wall superheat and three heat transfer components in an upward subcooled boiling flow. The QoIs over 12 different input heat fluxes are extracted from the report. Since the data provided in the report are averaged on the whole 10mm-by-10mm heat surface, the QoIs obtained from MCFD simulations in this work are also averaged in the same manner to match the data.

The closure relation that is pertinent to the boiling process is the wall boiling model which consists of the heat partition and the nucleation related empirical correlations. Thus the wall boiling closure relations are the focus of this scenario. It is also assumed that other closure relations including the interfacial forces have a minor impact on the wall heat transfer behavior and thus do not need to be considered in the UQ process in this case study. This assumption is based on the observation of the chosen boiling closure relations studied in this case, which relies only on one flow feature: the y^+ in near wall cell. The y^+ value is obtained along with the mesh study and is assumed to be independent from the wall boiling closure relations. The evaluation process can be summarized in Table 1.

Table 1. Summary of evaluations for wall boiling heat transfer scenario

| Scenario | QoIs | Varying input Condition | Closure relations studied |
|------------------------|-----------------------------------|--|--|
| Subcooled flow boiling | $T_{sup}, q_{Ev}, q_{Qu}, q_{Fc}$ | Applied wall heat flux: 500 ~ 2500 kW/m ² | Nucleation site density, Bubble departure diameter, Bubble departure frequency, Effective bubble area, Bubble growth waiting time, Convective heat transfer |

The wall boiling closure relations studied in this paper are based on the heat partitioning model proposed by (Kurul and Podowski,1991). The heat is partitioned into these three components, and each component is support by one to several empirical closure relations.

$$q_{wall} = q_{Ev} + q_{Qu} + q_{Fc} \quad (1)$$

The evaporation heat transfer is dependent on three nucleation correlations: the active nucleation site, the bubble departure diameter and bubble departure frequency:

$$q_{Ev} = \frac{\pi}{6} D_d^3 \rho_v f_d N_a h_{fg} \quad (2)$$

The nucleation site density model studied in this work is proposed by (Hibiki and Ishii,2003)

$$N_a = N_{avg} \left[1 - \exp\left(-\frac{\theta^2}{8\mu_{con}^2}\right) \right] \left[\exp\left(\frac{\lambda' g(\rho^+)}{R_c}\right) - 1 \right], \quad (3)$$

where

$$R_c = \frac{2\sigma \{1 + (\rho_g/\rho_f)\}/P_f}{\exp\{h_{fg}(T_g - T_{sat})/R T_g T_{sat}\} - 1} \quad (4)$$

$$f(\rho^+) = -0.01064 + 0.48246\rho^+ - 0.22712\rho^{+2} + 0.05468\rho^{+3} \quad (5)$$

$$\rho^+ = \log\left(\frac{\rho_l - \rho_g}{\rho_g}\right). \quad (6)$$

Here N_{avg} , μ_{con} and λ' are empirical parameters that represent the average cavity density, angle scaler, and cavity radius scaler respectively.

The bubble departure diameter model studied in this work is proposed by (Kocamustafaogullari, 1983):

$$D_d = d_1 \theta \left(\frac{\sigma}{g\Delta\rho}\right)^{0.5} \left(\frac{\Delta\rho}{\rho_g}\right)^{0.9} \quad (7)$$

The bubble frequency model studied in this work is proposed by (Cole, 1967)

$$f_d = \sqrt{\frac{4g(\rho_l - \rho_g)}{3D_d\rho_l}}. \quad (8)$$

The Quenching heat transfer is based on analytical analysis (Del Valle and Kenning, 1985), yet several terms in the expression are still depend on empirical parameters:

$$q_{qu} = A_b \frac{2}{\sqrt{\pi}} f_d \sqrt{t_{wait} \lambda_l \rho_l c_{p,l} (T_{sup} - T_l)}. \quad (9)$$

A_b in the expression is the effective bubble area fraction,

$$A_b = \max\left(\pi \left(a \frac{D_d}{2}\right)^2 N_a, 1.0\right), \quad (10)$$

and a is the bubble influence factor which is an empirical parameter. Moreover, t_{wait} is the waiting time between the bubble departure and the appearance of a new bubble at a given nucleation site. In this work, the model proposed by (Podowski et al., 1997) is selected:

$$t_{wait} = \frac{e}{f_d}, \quad (11)$$

where e is the waiting time coefficient, the suggested value is 0.8.

The forced convective heat transfer can be expressed as

$$q_{Fc} = (1 - A_b) h_l (T_{sup} - T_l), \quad (12)$$

where h_l is the heat transfer coefficient, which can be evaluated through the analysis of heat transfer in turbulent boundary layer flow. The wall function of turbulence model is applied which relates h_l to the turbulent Prandtl numbers and the dimensionless near-wall flow velocity. In this work, a simplified version of the correlation proposed by (Jayatilke, 1969) is adopted as

$$h_l = u_\tau \rho c_p \left[\text{Pr}_t \frac{1}{\kappa} \ln(Ey^+) + P \right]^{-1}, \quad (13)$$

where E and P are the empirical parameters from the wall function.

As noted from the empirical correlations discussed previously, the number of the empirical parameters is quite large but not all of them have clear physical meanings. Based on this, a preliminary parameter selection is processed to choose those with clear physical meanings for further UQ process. The prior uncertainties of those selected empirical parameters are determined based on expert judgment. The results are summarized in Table 2. “Non-informative” uniform distributions are assumed for all the parameters.

Table 2. Prior uncertainties of studied empirical parameters in wall boiling closures

| Empirical parameter | Physical meaning | Nominal value | Lower bound | Upper bound |
|---------------------|--|--------------------|--------------------|--------------------|
| N_{avg} | Averaged Nucleation site density coefficient | 4.72×10^5 | 4.72×10^4 | 4.72×10^6 |
| μ_{con} | Contact angle scaler | 0.722 | 0.4 | 3.14 |
| d_1 | Departure diameter constant | 0.0015 | 0.0005 | 0.003 |
| a | Effective bubble area factor | 1 | 0.5 | 2 |
| e | Bubble growth waiting time factor | 0.8 | 0.5 | 0.95 |
| E | Wall function Log law offset | 9.79 | 1 | 15 |
| P | Wall function coefficient | 0 | -9 | 9 |

2.2 Surrogate construction

As noted for the aforementioned closure relations, the wall boiling closure relations can be regarded as source terms that only loosely coupled with the conservative equations. Thus, a simplified physical based surrogate model is constructed for this case study. The structure of the simplified model is illustrated in Figure 2.

It can be found that the wall boiling closure relation can be regarded as a network of different correlations, which combine to form a non-linear equation with the constraint of a fixed and known value: the total wall heat flux. Following this structure, the wall superheat can be calculated by solving a non-linear equation using the Newton-Raphson method. Once the wall superheat is obtained, the heat transfer components can be calculated respectively.

For this simplified model, only one feature is required from the simulation of MCFD solver: the y^+ of the near wall cell. For this case, the y^+ is obtained and prescribed through the mesh study, which is performed before any cases are simulated in the solver. Since the wall function of the turbulence model is included for all the simulation in this work, the near wall y^+ should be greater than 30. A uniform mesh is chosen to meet this criterion through the mesh study. Based on the mesh setup, the y^+ is obtained and assumed to be independent of parameters of wall boiling closure relations.

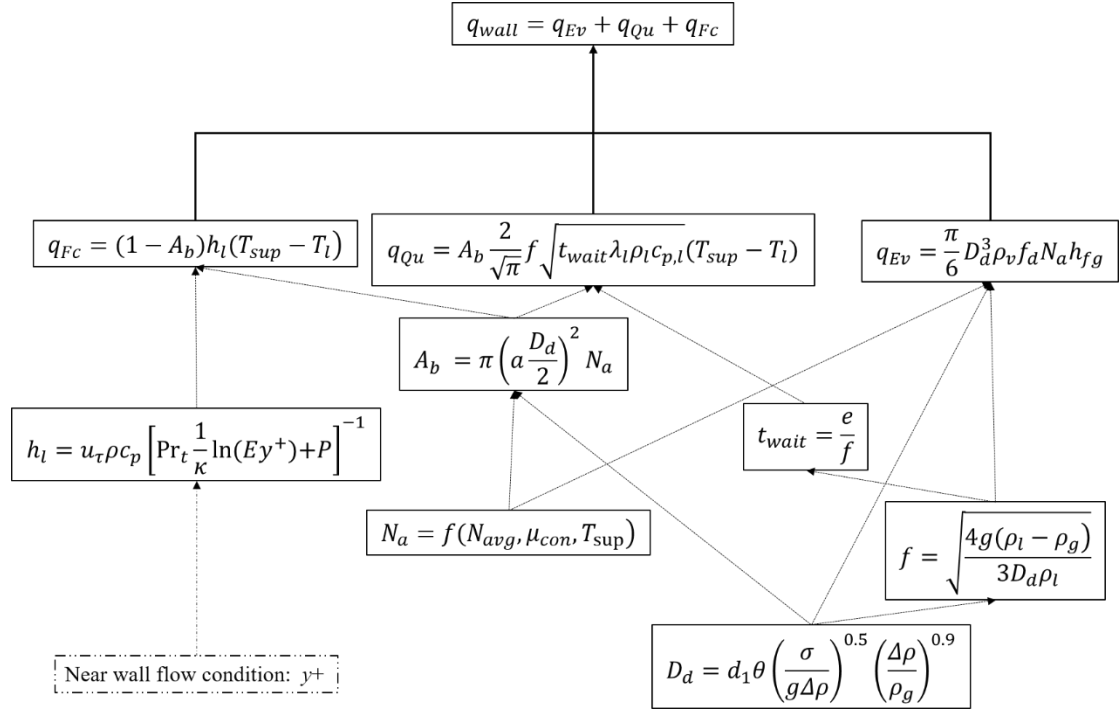


Figure 2. Structure of wall boiling closure relations in this case study

2.3 Sensitivity analysis

In this step, two methods of global sensitivity analysis (GSA) are performed. As previously discussed, the QoIs are the averaged quantities over the heating surface. In this step, those obtained QoIs are further integrated over the whole simulation domain to generate global responses quantity for GSA. The results of Morris Screening method are plotted in Figure 3.

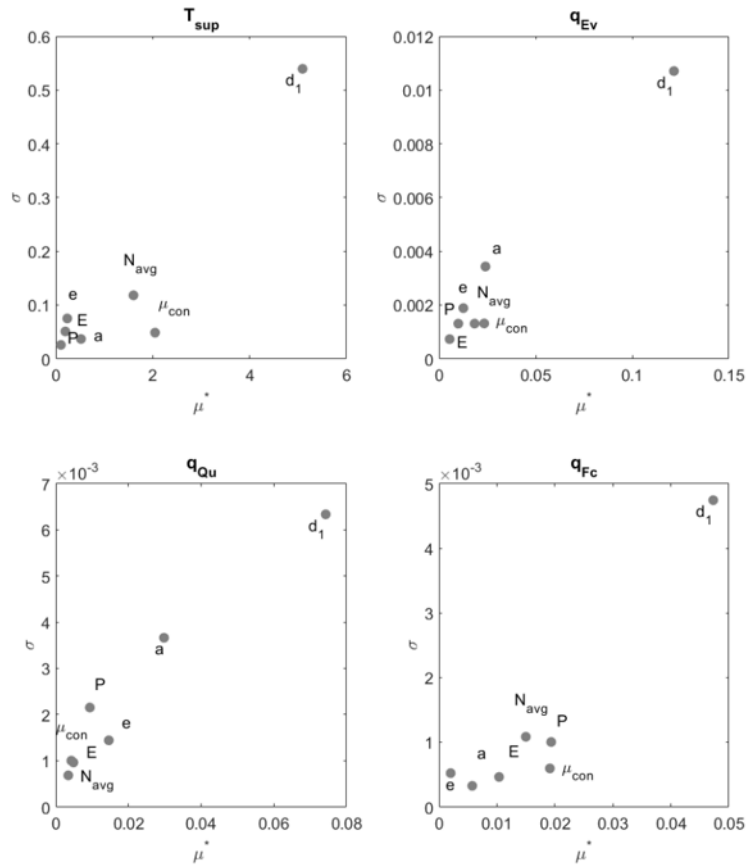


Figure 3. Morris screening measures for wall boiling empirical parameters

It can be observed that for all the QoIs, the bubble departure diameter constant d_1 is the most influential parameter. This is reasonable considering the fact that the evaporation heat transfer component is dependent on the third power of d_1 , while for other parameters the relationship is linear. For other parameters, the importance varies by different QoIs. For example, the nucleation site density constant N_{avg} has relatively strong influence on wall superheat, whereas the contact angle scaler μ_{con} has influence on wall superheat and convective heat transfer component. Moreover, the bubble effect area factor a plays a relatively important role on evaporation and quenching heat transfer components.

Morris screening is an efficient measurement method for GSA, but it cannot generate a quantitative measurement of the parameters sensitivity on the QoIs. The Sobol indices method, on the other hand, can generate indices that quantitatively measure the sensitivity of parameters on the QoIs, while is much more computationally expensive. The results of Sobol indices for the four QoIs are plotted in Figure 4.

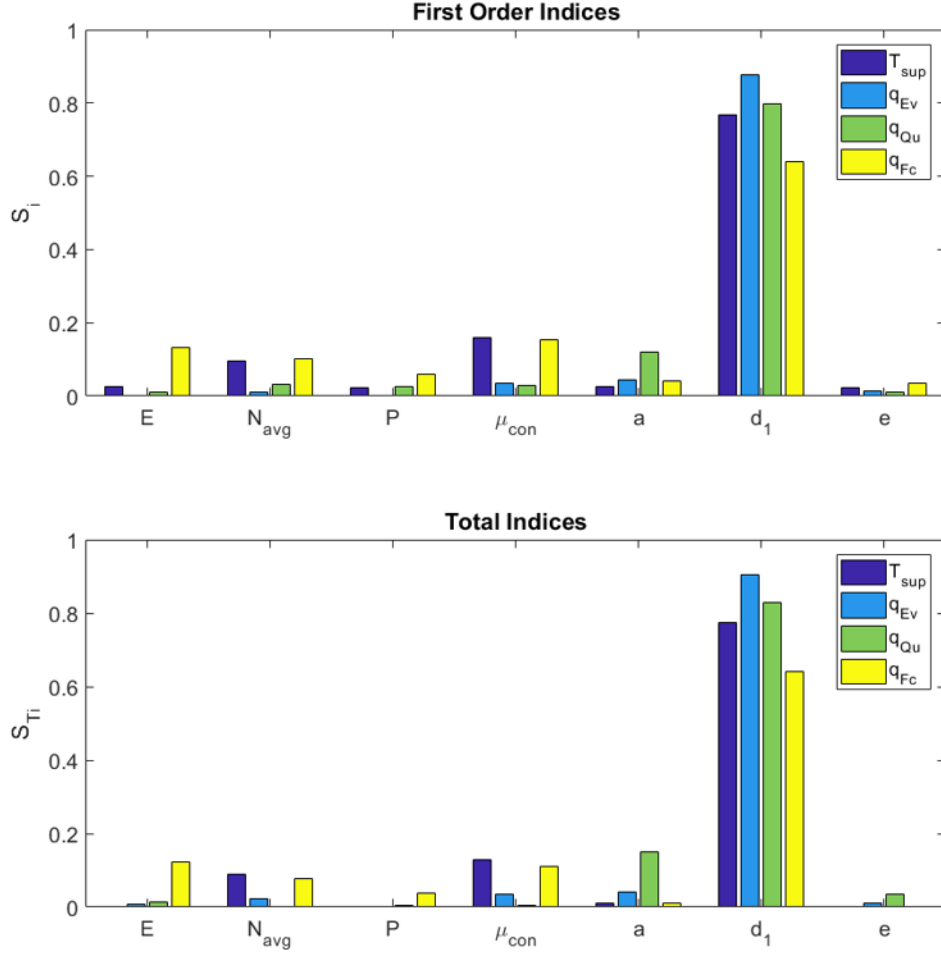


Figure 4. Sobol indices for wall boiling empirical parameters

It is noted in Figure 4 that the bubble departure diameter constant d_1 is the dominant parameter for all QoIs, the results of other parameters are also consistent with the Morris Screening method. Thus we can conclude that the GSA results from those two methods are consistent.

2.4 Parameter selection

As noted from GSA results, the most dominant parameter for all QoIs is d_1 . However, all other parameters are still influential to at least one QoI. There is no clear clue to rule out anyone of them. Moreover, preliminary MCMC sampling suggest that the parameter identifiability issue exists when inferring all the parameters together. Thus, the parameter selection algorithm proposed by (Banks et al., 2013) discussed in the first part paper is applied. Firstly, the rank of the sensitivity matrix is computed using singular value decomposition (SVD). The rank of the sensitivity matrix is found to be 4, which equals to the maximum number of identifiable parameters for the given closure relations with nominal parameter values. Then the selection score for all the possible combinations of parameters is calculated based on the proposed algorithm. This procedure is performed for all QoIs respectively. Some results are summarized in Table 3.

Table 3. Optimal selection scores for different QoIs

| Parameter combination | Selection score for T_{sup} | Selection score for q_{Ev} | Selection score for q_{Qu} | Selection score for q_{Fc} |
|--------------------------|-------------------------------|------------------------------|------------------------------|------------------------------|
| (a, d_1, e, E) | 103.36 | 1.446E+06 | 3.047E+06 | 1.398E+07 |
| (a, μ_{con}, e, P) | 133.76 | 1.823E+06 | 8.679E+06 | 4.772E+06 |
| (a, μ_{con}, d_1, e) | 90.55 | 6.518E+05 | 4.630E+06 | 6.548E+06 |

It can be found from the results that for different QoI, the parameter selection with minimum selection score is different, in this sense, trade-off needs to be made between different QoIs. In a preliminary MCMC, single-value dependence between μ_{con} and d_1 is observed, which is undesired for the Bayesian inference. Thus in this work, the parameter combination (a, d_1, e, E) is selected for the Bayesian inference. A more robust selection criterion for multiple QoIs is desired for future work.

2.5 Uncertainty quantification

In the step of uncertainty quantification, the modular Bayesian is applied, which firstly evaluate the model form uncertainty using Gaussian process while fix the parameters at their nominal values. In this case, the full datasets are divided into three parts: 6 datasets are used to evaluate the model form uncertainty, 5 datasets are used for model parameter uncertainty inference, while 1 dataset is left for testing. The decomposition is summarized in Table 4.

Table 4. Boiling datasets decomposition for different purposes

| Datasets decomposition | Input heat flux (kW/m ²) |
|--|--------------------------------------|
| Model form uncertainty evaluation datasets | 500, 1000, 1500, 2200, 2400, 2450 |
| Parameter uncertainty evaluation datasets | 750, 1250, 1750, 2100, 2300 |
| Testing dataset | 2000 |

In this work, the QoIs measured over the surface are averaged, thus the model form uncertainty term is spatially independent and can be expressed by a single variant GP: $\delta(q_{wall}) \sim GP(q_{wall})$. Six datasets are used for evaluating the model form uncertainty. The exponential kernel is selected as the kernel function of GP. The hyperparameters of the kernel are evaluated using the MAP method. The obtained results are plotted in Figure 5.

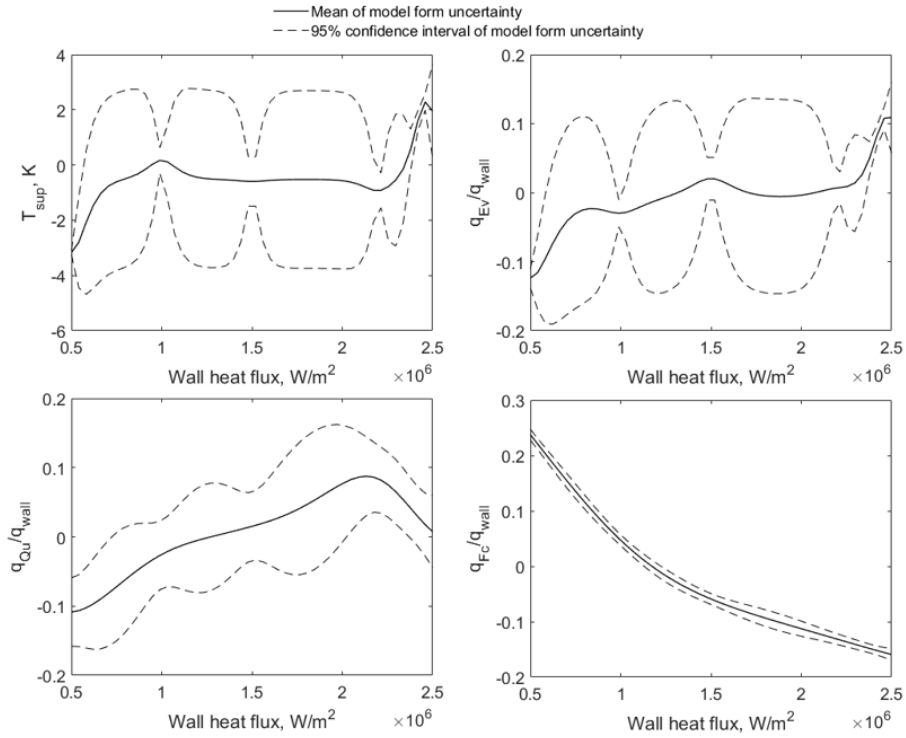


Figure 5. Model form uncertainty $\delta(q_{wall})$ for different QoIs

It can be found from Figure 5 that the T_{sup} has small model form uncertainties, with exceptions under high and low heat flux conditions. The other QoIs have significant discrepancy between model predictions and experimental measurements. To some extent, this is expected considering the fact that when the wall boiling closure relations were proposed, the only measurable data was the wall superheat. Thus, the wall boiling closure relations have already been compared against many different wall superheat measurements, and can give wall superheat predictions with reasonable accuracy. On the other hand, the heat partitioning prediction lacks comparison due to the lack of experimental measurements, thus the existent significant model form uncertainty cannot be identified if only takes the wall superheat into consideration. In this practice, the model form uncertainties can be identified under the TMDI approach by “learning” from the multiphysics measurement.

Once the parameters for inverse UQ are selected, the MCMC method is applied for Bayesian inference. The MCMC has been applied to similar applications such as the inverse UQ on turbulence model (Edeling et al., 2014) and fluidized-bed gasifier simulations (Gel et al., 2016). The Delayed Rejection Adaptive Metropolis (DRAM) algorithm proposed by (Haario et al., 2006) is applied. There are two features of DRAM, one is delayed rejection, which means if a candidate is rejected in the sampling process, an alternate candidate is constructed to induce greater mixing. The other is adaption, which means the covariance matrix of the parameters is continuously updated using the accepted candidates.

The purpose of the MCMC is to construct stationary distribution of a Markov chain that equals to the posterior distribution of the parameter. In practice, the first 5000 samples from the chain are disregarded to ensure the convergence (or so-called “burn-in”) of the following chains.

Moreover, for the “burned-in” chain, only every 10th elements are kept in order to reduce the auto-correlation of the chain as a requirement of the stationary distribution.

The processed sample chain for all selected parameters, and their autocorrelations are plotted in Figure 6. Good mixing and the fast decay of auto-correlations for all parameters can be observed which indicate the process chain can be regarded as the stationary distributions of the Markov chains.

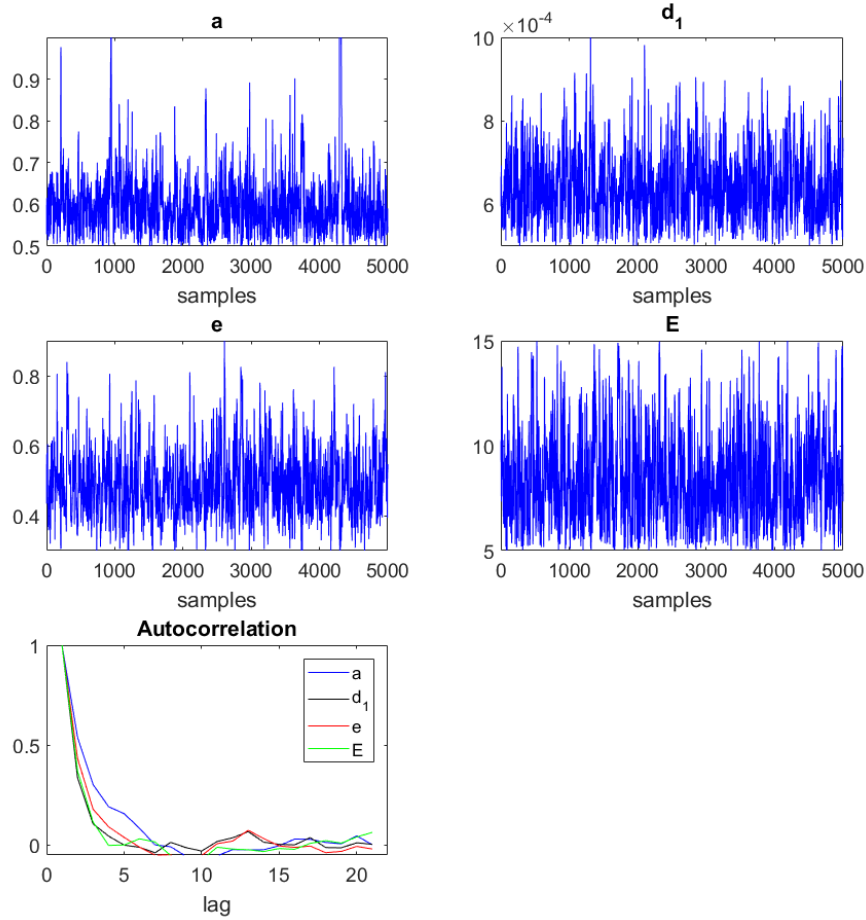


Figure 6. MCMC sample traces and auto-correlations of wall boiling closure relation parameters

The marginal and pair-wise joint distributions of the four parameters are plotted in Figure 7. Light correlation between d_1 and e is observed, while they come from different closure relations. This suggests that with the TDMI approach, which takes all closure relations and all QoIs of the solver into consideration simultaneously, the potential interaction between different phenomena can be identified. The statistics of the parameter distribution are summarized in Table 5.

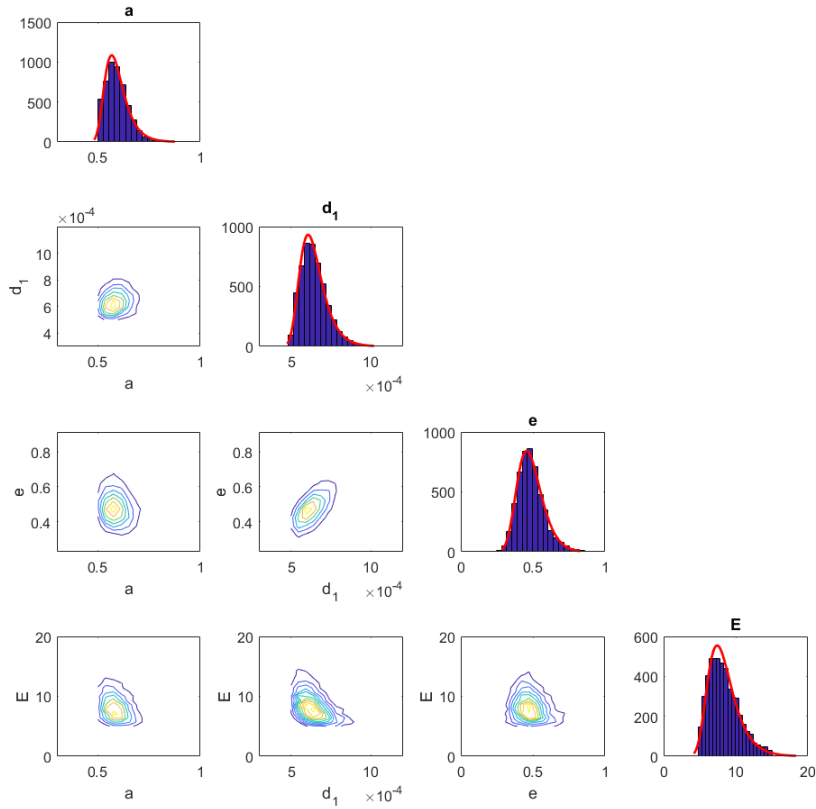


Figure 7. Marginal and pair-wise joint distributions of selected empirical parameters

Table 5. posterior statistics of selected empirical parameters

| Parameter | Mean | Standard deviation | 95% Confidence interval |
|-----------|-----------------------|-----------------------|--|
| a | 0.5943 | 0.0743 | [0.4523, 0.7445] |
| d_1 | 6.42×10^{-4} | 7.98×10^{-5} | $[4.85 \times 10^{-4}, 7.98 \times 10^{-4}]$ |
| e | 0.5135 | 0.0916 | [0.3520, 0.7110] |
| E | 8.3839 | 2.1374 | [4.2580, 12.6366] |

Once the posterior distributions of the parameters are obtained, the uncertainties of QoIs can be estimated by propagating the posterior distributions through the solver, the previously obtained model form uncertainty can be added to the obtained QoIs as a correction term. The obtained results are displayed in Figure 8.

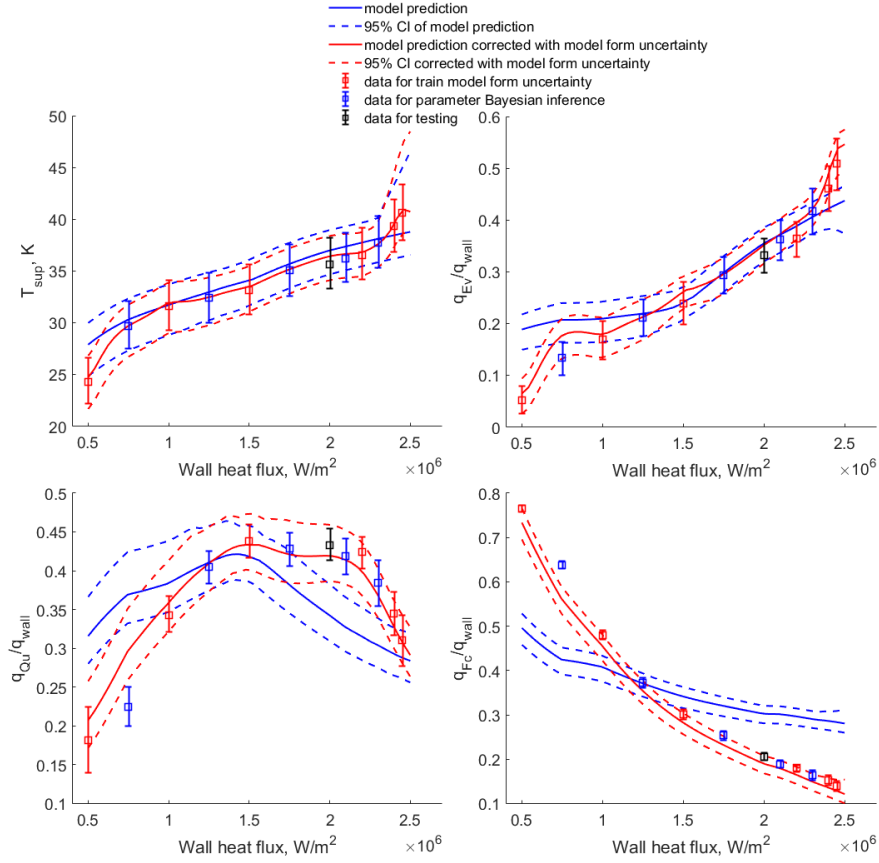


Figure 8. 95% confidence intervals (CIs) for different QoIs from wall boiling closure relations

It can be observed from Figure 8 that the predictions of T_{sub} and q_{Ev} are generally in good agreement with the whole dataset. However, q_{Qu} is overestimated in low heat flux region while is underestimated in high heat flux region, and q_{FC} demonstrates the opposite trend. Moreover, for all QoIs, if takes the model form uncertainty into consideration, the model prediction will be in good agreement with the experimental measurement for all the input conditions. Moreover, since the model form uncertainty is constructed using Gaussian Process (GP) which treat the input condition as variable, it can be interpolated to any unmeasured wall heat flux. In this sense, the applicable range of the UQ results is $500 \text{ kW/m}^2 \sim 2500 \text{ kW/m}^2$, which basically covers normal nucleate boiling regime.

2.6 Validation metrics

In this work, two different types of validation metrics are calculated: the confidence interval (Oberkampf and Barone,2006) and the area metric (Ferson and Oberkampf,2009). The confidence intervals for the QoIs from wall boiling closure relations are plotted in Figure 9.

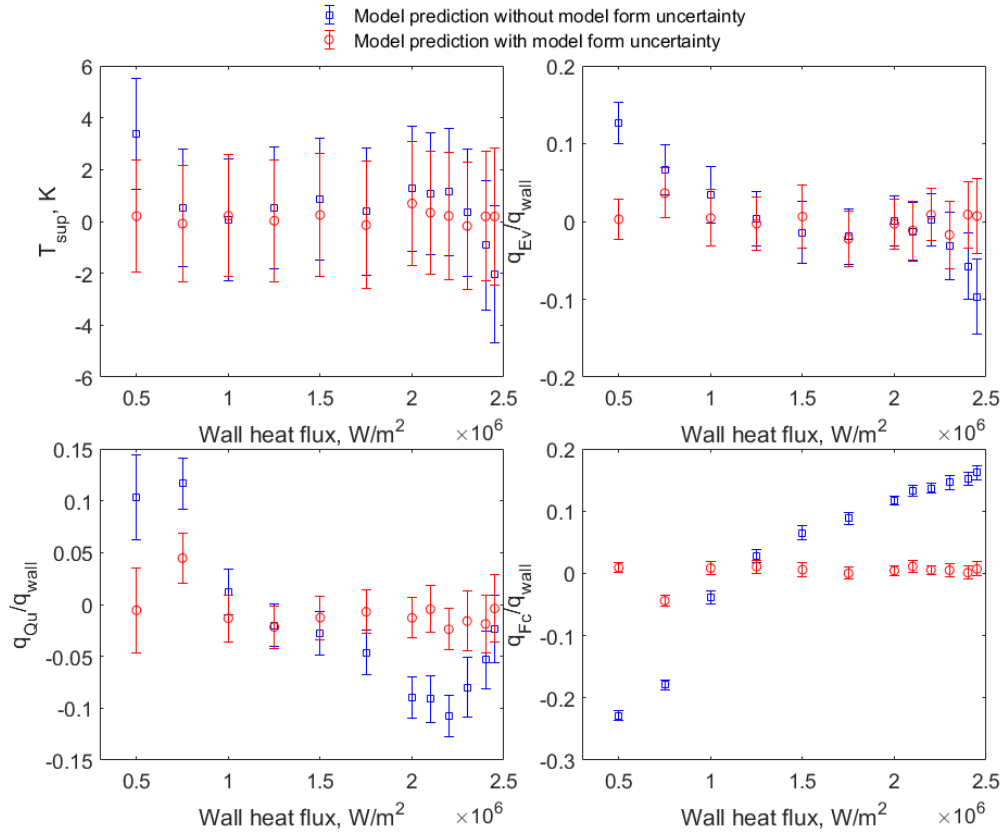


Figure 9. Confidence intervals for different QoIs from wall boiling closure relations

If only consider the pure model prediction, it can be found the confidence intervals of T_{sup} are close to or covers zero, with exceptions in 500kW/m^2 and 2500kW/m^2 . This suggests that the model prediction of T_{sup} is in good agreement with the experimental measurement. For other three QoIs, most of the confidence intervals deviate from zero. This indicates that the true error between model predictions and data are significant. Taking the q_{Fc} as an example, it can be observed that the wall boiling closure relation significantly underestimates the convective heat transfer for low heat flux cases while overestimating it for high heat fluxes. On the other hand, it can be observed that with the consideration of model form uncertainty, the errors are significantly reduced for almost all the cases. Such improvement indicates that the wall boiling closure relations has intrinsic model form uncertainty, and such model form uncertainty can be successfully evaluated through the proposed “Modular Bayesian” approach.

The advantage of confidence interval is it has very clear physical interpretation while also easy to implement. For example, the 95% confidence interval can be interpreted as we are 95% confident that the true error of QoI predicted by the solver is within the given interval. Such interpretation can be directly applied in the design and safety analysis for a certain engineering problem. One disadvantage of confidence interval, however, is only the mean of the QoIs predicted by solver is considered and the interval contains only statistics from the uncertainty of experimental data. In other words, the confidence interval fails to consider the full uncertainty of the solver predictions and the experimental data.

The area metric, on the other hand, compensates for the disadvantage of confidence interval by comparing the discrepancy between the cumulative distribution functions (CDFs) of the experimental data and the solver prediction. The results of area metric are plotted in Figure 10. It should be noted that every single point displayed in the figure represent the integrated area between the two CDFs mentioned above, a large value of area metric suggest large difference between the CDFs of model prediction and experimental data.

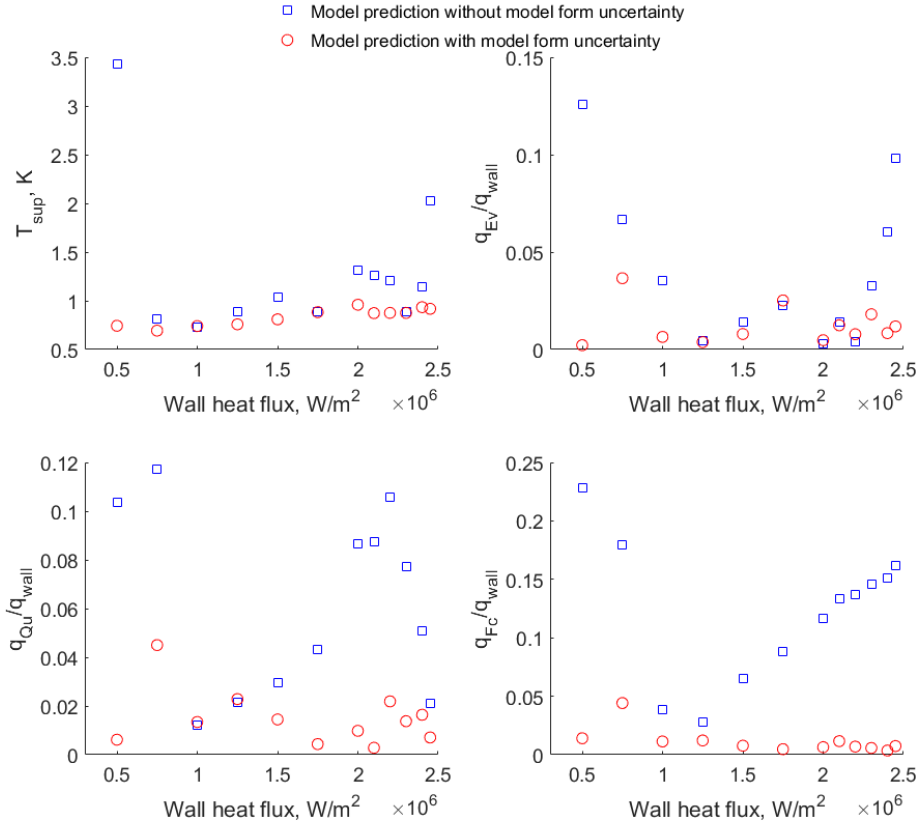


Figure 10. Area metrics for different QoIs from wall boiling closure relations

It can be found that for the pure model prediction, T_{sup} has small area metrics, with exceptions in 500kW/m^2 and 2500kW/m^2 . For the other three QoIs, the pure model predictions have significant difference with experimental data. With model form uncertainty is accounted for, the results are significantly improved. In this sense, the two validation metrics are consistent. Another advantage of area metric is that it has several properties as suggested by (Ferson et al., 2008) that make it mathematically well behaved and well understood. Such properties can be expressed as following for CDFs of two random variables X and Y :

- Non-negativity: $d(X, Y) \geq 0$
- Symmetry: $d(X, Y) = d(Y, X)$
- Triangle inequality: $d(X, Y) + d(Y, Z) \geq d(X, Z)$
- Identity of indiscernible: $d(X, Y) = 0$ if and only if $X = Y$

On the other hand, there are also two disadvantages of the area metric. One is that the area metric is much more complicated to calculate compared with confidence interval. It also puts

higher requirement for the data quality, requires not just the statistics of the data such as its mean and variance, but the full distribution. This usually requires measuring the same quantities multiple times. The other disadvantage is that the area metric measures the absolute difference between the solver predictions and the data. Thus it cannot discern whether the solver is overestimate or underestimate the QoIs. Thus, it is suggested to calculate both validation metrics for a comprehensive evaluation of the agreement between the solver prediction and experimental data.

3. Case study II: VUQ on flow dynamics

3.1 Solver evaluation and data collection

The MCFD's performance on flow dynamics in the context of upward adiabatic bubbly flow is studied in this case. The reason to choose this scenario is the relatively rich experimental data. Several experimental investigations can be found from literature, which includes a series measurement of the phasic velocity, the void fraction, and the bubble dynamics. Representative works include (T. J. Liu and Bankoff,1993), (Leung et al., 1995), and many more summarized in (Lin and Hibiki,2014).

A simplified case is considered which focuses on only two QoIs: the void fraction and gas velocity. Based on the idea of TDMI, the experimental data from different conditions are taken into consideration simultaneously. Thus, the experiments conducted by (Leung, 1997) are chosen as the datasets, from which eight datasets of different inlet conditions are extracted. The summary of evaluations is summarized in Table 6. For the VUQ process, the uncertainty of data is important. However, the detail uncertainty analysis is not included in the original literature. In this work, the conservative estimation based on an incomplete error analysis from the original literature is adopted, the uncertainty for all QoIs is assumed to be 10%.

Table 6. Summary of evaluations for interfacial momentum closure relations

| Scenario | QoIs | Varying input Condition | Closure relation studied |
|-----------------------|---|--|--|
| Adiabatic bubbly flow | spatial distributions of α , U_1 | j_g from 0.09 – 0.48 m/s, j_l from 0.64 – 2.0 m/s | drag force, lift force, turbulent dispersion force, virtual mass force, wall lubrication force |

The interfacial force coefficients are investigated. For drag and lift force, there are many semi-mechanistic correlations for the coefficients. In this work, a simplified version is used which assumes those coefficients are independent with the flow condition and can be expressed by constant values. Besides the interfacial forces, the bubble size also has a significant influence on the bubbly flow simulation. The state of the art method for bubble size prediction is to solve

the interfacial area concentration equation along with the conservation equations. This approach, however, includes more parameters and requires many more extra sampling runs in the MCFD solver. Considering the limitation of computational resources, in this first demonstration case, a simplified assumption for bubble size was made. The bubble size is set to be a constant whose value equals to the inlet bubble size. Thus, only the interfacial momentum closure relations are studied and the model selected is summarized in Table 7. The prior uncertainties of the interfacial force coefficients are summarized in Table 8. The uniform uncertainties are assumed for those parameters, as the same to the Case Study I.

Table 7. Summary of the studied interfacial momentum closure relations

| Force type | Expression | Parameter studied |
|--|---|-------------------|
| Drag force | $\mathbf{M}_g^D = -\frac{3}{4} \frac{C_d}{D_s} \rho_l \alpha \ \mathbf{U}_g - \mathbf{U}_l\ (\mathbf{U}_g - \mathbf{U}_l)$ | C_d |
| Lift force | $\mathbf{M}_g^L = C_l \rho_l \alpha (\mathbf{U}_g - \mathbf{U}_l) \times (\nabla \times \mathbf{U}_g)$ | C_l |
| Wall lubrication force (Antal et al., 1991) | $\mathbf{M}_g^{WL} = -f_{WL}(C_{wl}, y_w) \alpha \rho_l \frac{\ \mathbf{U}_r - (\mathbf{U}_r \cdot \mathbf{n}_w) \mathbf{n}_w\ ^2}{D_s} \mathbf{n}_w,$ $f_{WL}(C_{wl}, y_w) = \max\left(-0.2 C_{wl} + \left(\frac{C_{wl}}{y_w}\right) D_s, 0\right)$ | C_{wl} |
| Turbulent dispersion force (Gosman et al., 1992) | $\mathbf{M}_g^{TD} = -\frac{3}{4} \frac{C_D}{D_s} \frac{v_l^t}{\sigma^t Pr_l^t} \rho_l \ \mathbf{U}_g - \mathbf{U}_l\ \nabla \alpha$ | σ^t |
| Virtual mass force (Auton et al., 1988) | $\mathbf{M}_g^{VM} = -C_{vm} \rho_l \alpha \left(\frac{D\mathbf{U}_g}{Dt} - \frac{D\mathbf{U}_l}{Dt} \right)$ | C_{vm} |

Table 8. Prior uncertainties of parameters in interfacial momentum closure relations

| empirical parameter | Nominal value | Lower bound | Upper bound |
|---------------------|---------------|-------------|-------------|
| C_d | 0.6 | 0.44 | 1.0 |
| C_l | 0.03 | -0.05 | 0.1 |
| C_{wl} | 0.05 | 0.03 | 0.08 |
| C_{vm} | 0.5 | 0.3 | 1.0 |
| σ^t | 0.9 | 0.6 | 1.2 |

To match the experimental measurement, the studied QoIs are set to be the distributions of void fraction and the gas velocity along the radial direction of the tube at ($z/D = 62$).

3.2 Surrogate construction

The surrogate model is constructed using Gaussian Process. There are eight datasets with different liquid and gas superficial velocities. Each case contains detailed 13 radial distributions of void fraction and gas velocity. Thus, the output QoIs can form a high dimensional vector. The length of the output QoIs is $8 \times 13 \times 2 = 208$. It is very inefficient to construct 208 separate GPs for the QoIs, thus the dimension reduction based on PCA is performed for this case.

Firstly, the MCFD simulations are performed with perturbed interfacial force coefficients sampling from Latin hypercube sampling. A total 64 samples are generated and run in the MCFD solver, among which 56 samples are used for surrogate construction and 8 samples are used for cross-validation.

Considering the high dimensionality of the outputs, the principal component analysis (PCA) applied for dimensionality reduction; the detailed algorithm is discussed in Appendix.B of the Part I paper. The void fraction and gas velocity simulation results are centered and scaled according to the inlet conditions, then stacked to create a matrix to which PCA is applied.

The results of the PCA applied to the combined void fraction and fluid temperature predictions are shown in Figure 11. It can be observed that up to 99.5% of the total variances can be explained by the first 8 principal components (PCs).

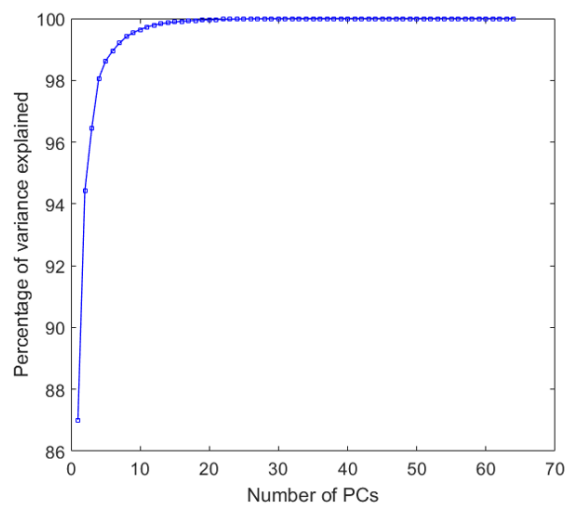


Figure 11. Accumulative percentage of variances explained by PCs

Based on the PCA results, the first 8 PCs are selected for constructing surrogate, this reducing the dimension of outputs from 208 to 8. The variations of the 8 PCs for one condition are summarized in Figure 12.

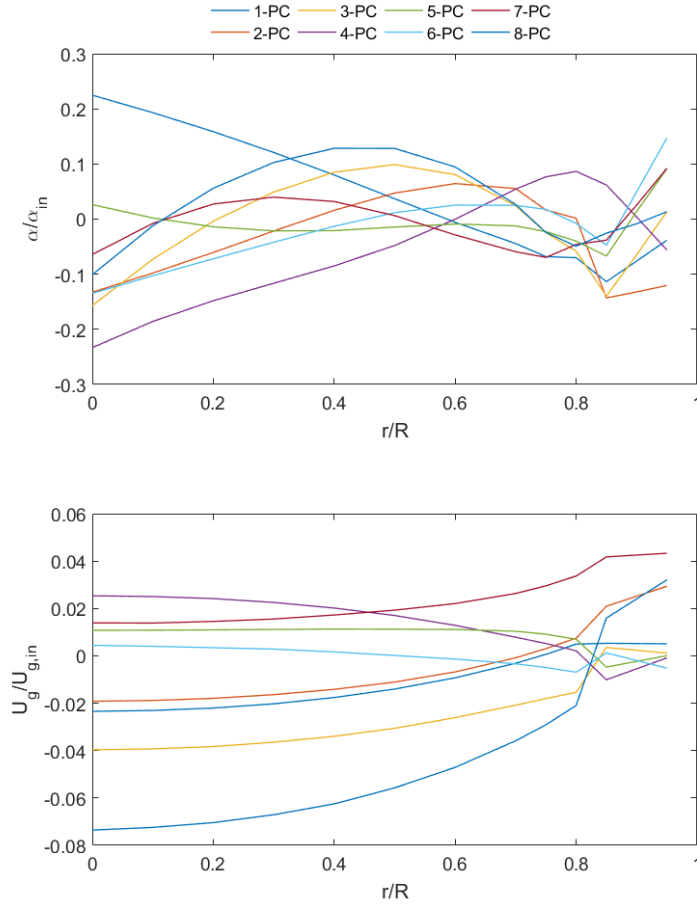


Figure 12. Variations of two QoIs captured by 8 PCs ($j_g = 0.29$ m/s, $j_l = 1.1$ m/s)

The GP surrogate is constructed for the 8 PCs, respectively. The constructed GP surrogate is an approximation of the original MCFD solver, whose accuracy should be evaluated. In this work, the cross validation is performed for the accuracy assessment. The procedure of cross-validation is done through the following steps:

- Randomly divide the sampled test case results into k groups of the same size.
- Construct the surrogate with $k-1$ groups of results and left 1 group as validation set.
- Repeat the previous step k times, in each time a different group is treated as a validation set.
- Average the obtained results from the k evaluations.

The comparisons of PC scores between MCFD simulations and GP predictions are plotted in Figure 13, where an accurate GP prediction should fall into or very close to the diagonal line in the plot. It can be found from the figure that the GP surrogate predictions are in good agreement with original MCFD simulations for most of the PC scores. Except for 3rd and 7th score which have some moderate discrepancies.

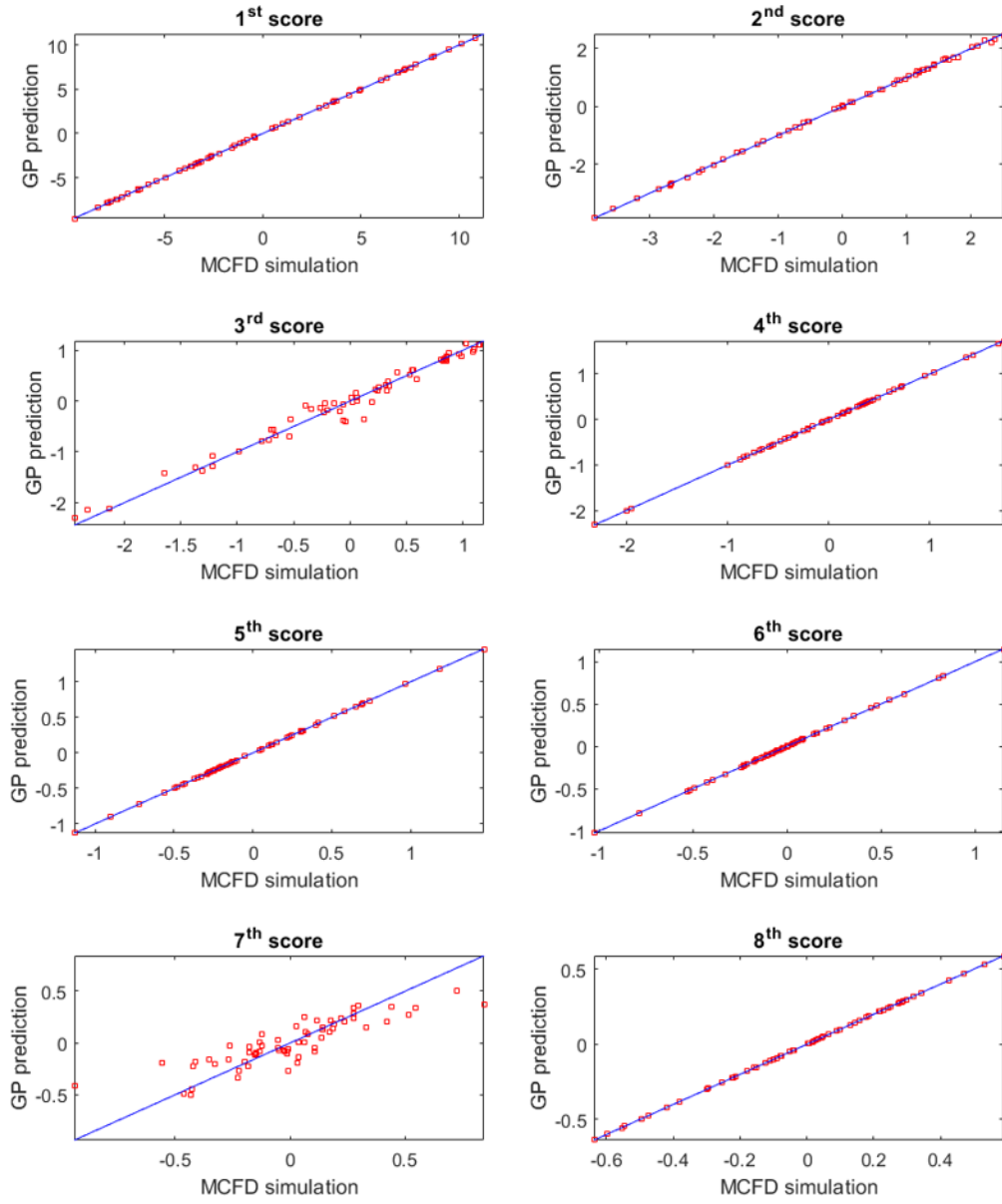


Figure 13. Comparison of PC scores between MCFD simulations and GP predictions

The averaged accuracy of surrogate can be estimated with the mean square error, the results for all the PCs are summarized in Table 9.

$$\text{MSE} = \frac{1}{N} \sum_{i=1}^N (\hat{y}_i - y_i^M)^2 \quad (14)$$

Table 9. Cross validation results

| PC scores | MSE |
|-----------------------|------------|
| 1 st score | 6.8542e-4 |
| 2 nd score | 0.0012 |
| 3 rd score | 0.0169 |
| 4 th score | 6.4328e-9 |
| 5 th score | 3.7789e-09 |
| 6 th score | 1.2514e-9 |
| 7 th score | 0.0240 |
| 8 th score | 3.0624e-09 |

The results confirm the qualitative observation from Figure 13, that the 3rd and 7th PC score has relative large MSE, but still in the acceptable range. It should be noted that both the GP surrogate and the PCA would inevitably introduce additional uncertainties. A rough estimate of these uncertainties can be made by comparing the differences between original solver predictions and the predictions given by surrogate. For most predictions, the difference between surrogate predictions and the original MCFD solver is less than 1%. However, extreme cases exist for predictions with near zero values where differences can be around 10%. It is also worth noting that it is still unclear how to estimate the uncertainty introduced by the statistical methods over the whole validation domain. In this work, we assume the uncertainties introduced by statistical methods is trivial compared to the model parameter uncertainty and model form uncertainty thus can be neglected.

3.3 Sensitivity analysis

Similar to the first case study, the solver predictions are averaged to generate a global response for the GSA. This averaging process indicates that the void fraction and velocity in different locations under different flow conditions are treated with equal importance. Thus two globally averaged quantities are analyzed using two GSA methods: the void fraction and gas velocity.

The GSA results using Morris Screening method are displayed in Fig. It can be found that for both QoIs, only three parameters are influential and their importance can be ranked as: $C_l > C_{wl} > C_d$. While the virtual mass force coefficient C_{vm} and turbulence dispersion coefficient σ^t has less influence on both of the QoIs.

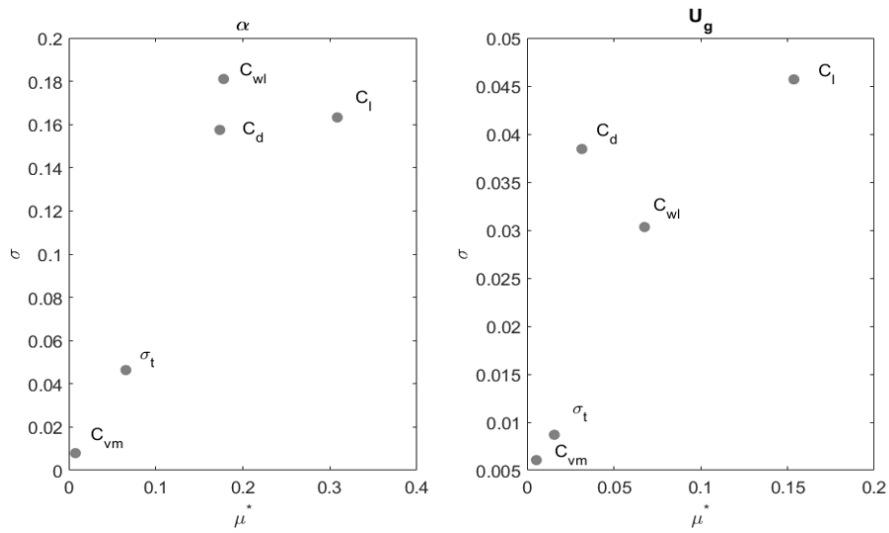


Figure 14. Morris screening measures for interfacial force coefficients

The Sobol indices plotted in Figure 15 is consistent with the Morris screening results, both the first order indices and total indices confirmed the same importance order.

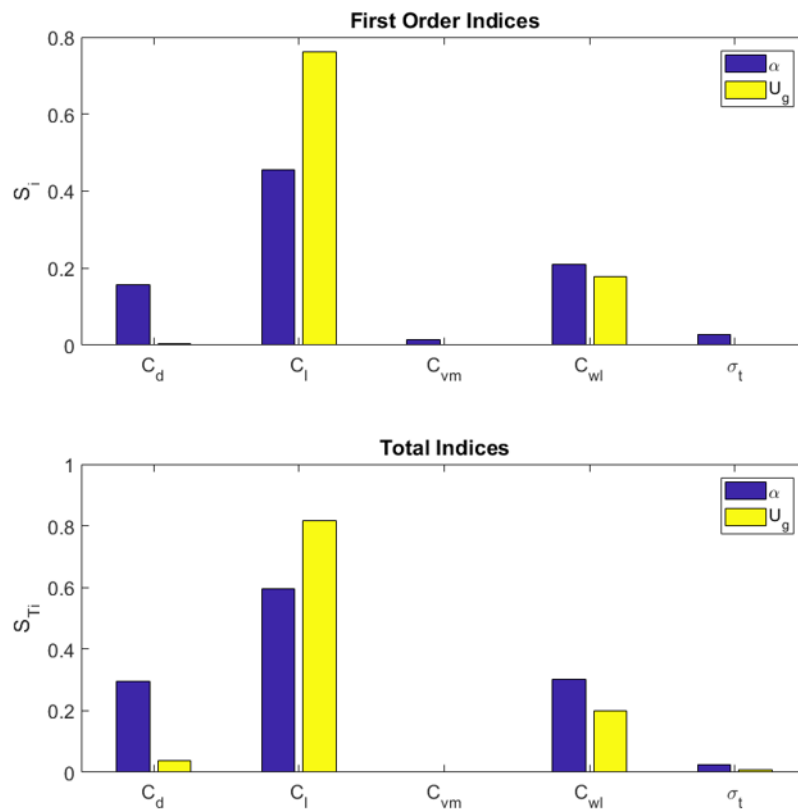


Figure 15. Sobol indices for interfacial force coefficients

There are only three influential parameters and the preliminary MCMC result shows no parameter identifiability issue. Thus there is no need to perform the parameter selection

algorithm. The three parameters are directly applied for the Bayesian inference for uncertainty quantification.

3.4 Uncertainty quantification

The model form uncertainty is evaluated using Gaussian process. The hyperparameters of the kernel function are evaluated using the MAP method. Unlike the first case study, the QoIs in this case is a spatial distribution, and there are two inlet conditions. Thus the model form uncertainty term is modeled by a multi-variant GP: $\delta(r/R, j_g, j_l) \sim GP(r/R, j_g, j_l)$. Due to the limitation of available datasets, 4 datasets are used for model form uncertainty evaluation, while 3 are used for model parameter uncertainty evaluation, and one dataset is left for testing. The decomposition is summarized in Table 10. The model form uncertainty distribution as a function of inlet superficial velocities at one location are plotted in Figure 16. It can be observed that the model form uncertainty of U_g at this location is negative over the whole input space, this suggest U_g is overestimated for all cases at this location.

Table 10. Flow dynamics datasets decomposition for different purposes

| Datasets decomposition | Inlet phasic superficial velocities (j_g, j_l) (m/s) |
|--|---|
| Model form uncertainty evaluation datasets | (0.16,0.64), (0.09,2.0), (0.16,2.0), (0.48,2.0) |
| Parameter uncertainty evaluation datasets | (0.09,0.64), (0.29,1.1), (0.29,2.0) |
| Testing dataset | (0.09,1.1) |

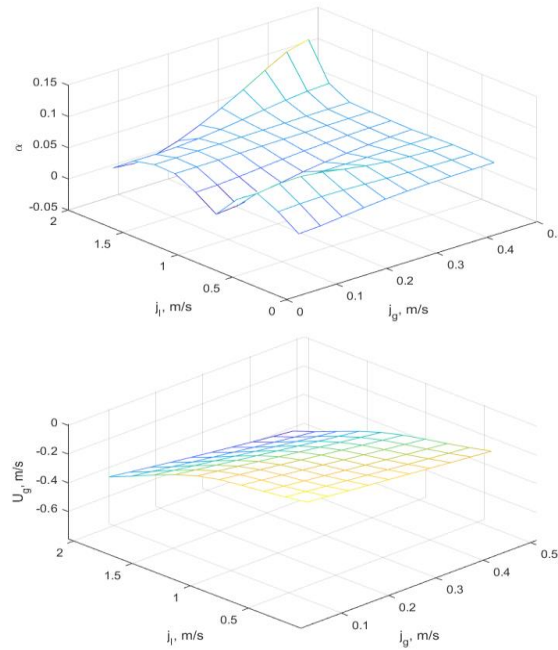


Figure 16. Model form uncertainty distribution at $r/R = 0.55$

For the inverse UQ on model parameters, the same process discussed in section 2.5 Uncertainty quantification is applied. The processed sample chain for all selected parameters and the autocorrelations of them are plotted in Figure 17. Good mixing and the fast decay of auto-correlations for all parameters can be observed.

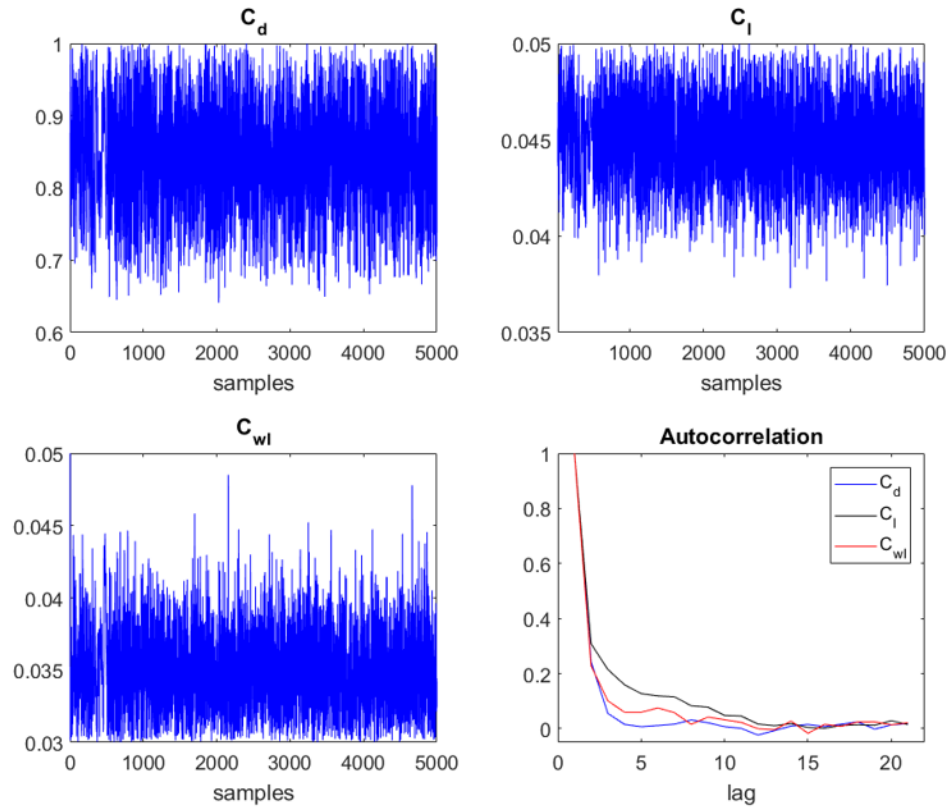


Figure 17. MCMC sample traces and auto-correlations of selected interfacial force coefficients

The obtained samples can be used to construct the stationary distribution of the Markov chain which can be regarded as the posterior distributions of the parameters. The obtained marginal and point-wise distributions of the three parameters are plotted in Figure 18. The statistics of the parameter distribution are summarized in Table 11. It can be observed that there is a correlation between C_l and C_{wl} . Generally speaking, large value of C_l will result a large value of C_{wl} . This again indicates TDMI can detect the possible interaction between different closure relations.

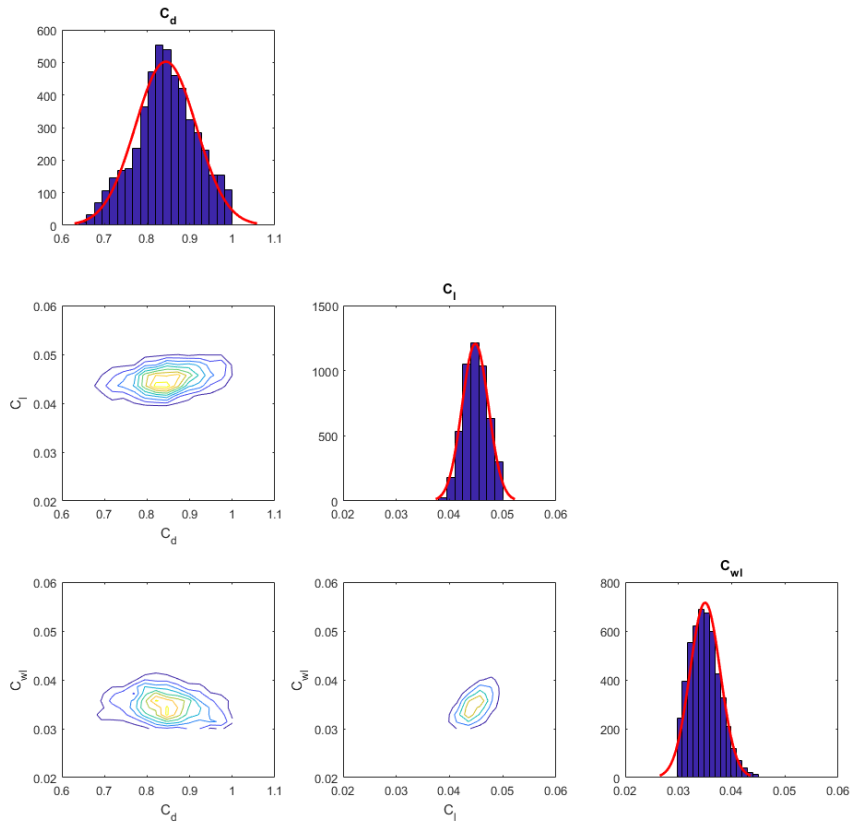


Figure 18. Marginal and pair-wise joint distributions of selected interfacial force coefficients

Table 11. Summary of posterior distributions of the influential interfacial force coefficients

| Parameter | Mean | Standard deviation | 95% Confidence interval |
|-----------|--------|--------------------|-------------------------|
| C_d | 0.8440 | 0.0711 | [0.6977, 0.9788] |
| C_l | 0.0448 | 0.0025 | [0.0403, 0.0492] |
| C_{wl} | 0.0350 | 0.0029 | [0.0304, 0.0412] |

Once the parameter uncertainties and model form uncertainties are obtained, the uncertainties of QoIs, with and without model form uncertainty, can be evaluated. The 95% predictive intervals of QoIs are plotted in Figure 19, Figure 20, Figure 21, which represent the model form uncertainty evaluation case, parameter uncertainty evaluation case and the test case respectively.

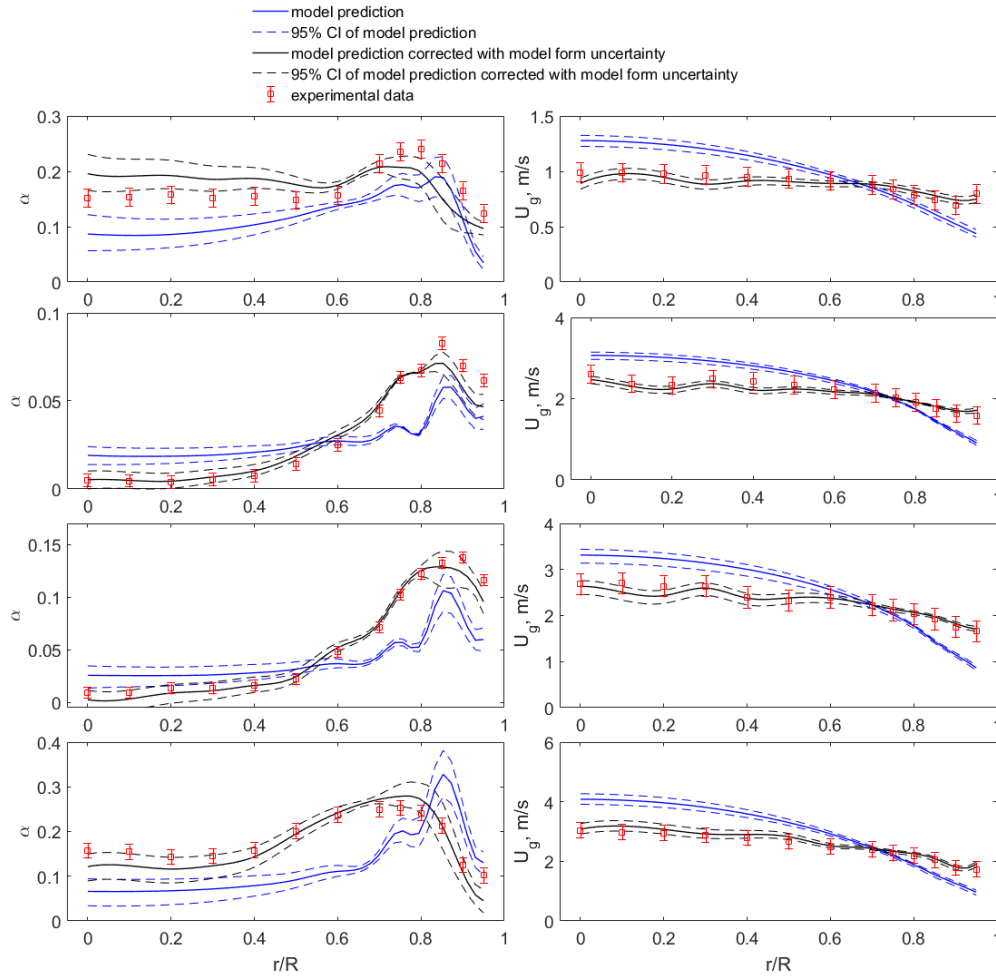


Figure 19. 95% confidence intervals of QoIs for model form uncertainty evaluation cases (first row: $j_g = 0.16$ m/s, $j_l = 0.64$ m/s; second row: $j_g = 0.09$ m/s, $j_l = 2.0$ m/s; third row: $j_g = 0.16$ m/s, $j_l = 2.0$ m/s; fourth row: $j_g = 0.48$ m/s, $j_l = 2.0$ m/s)

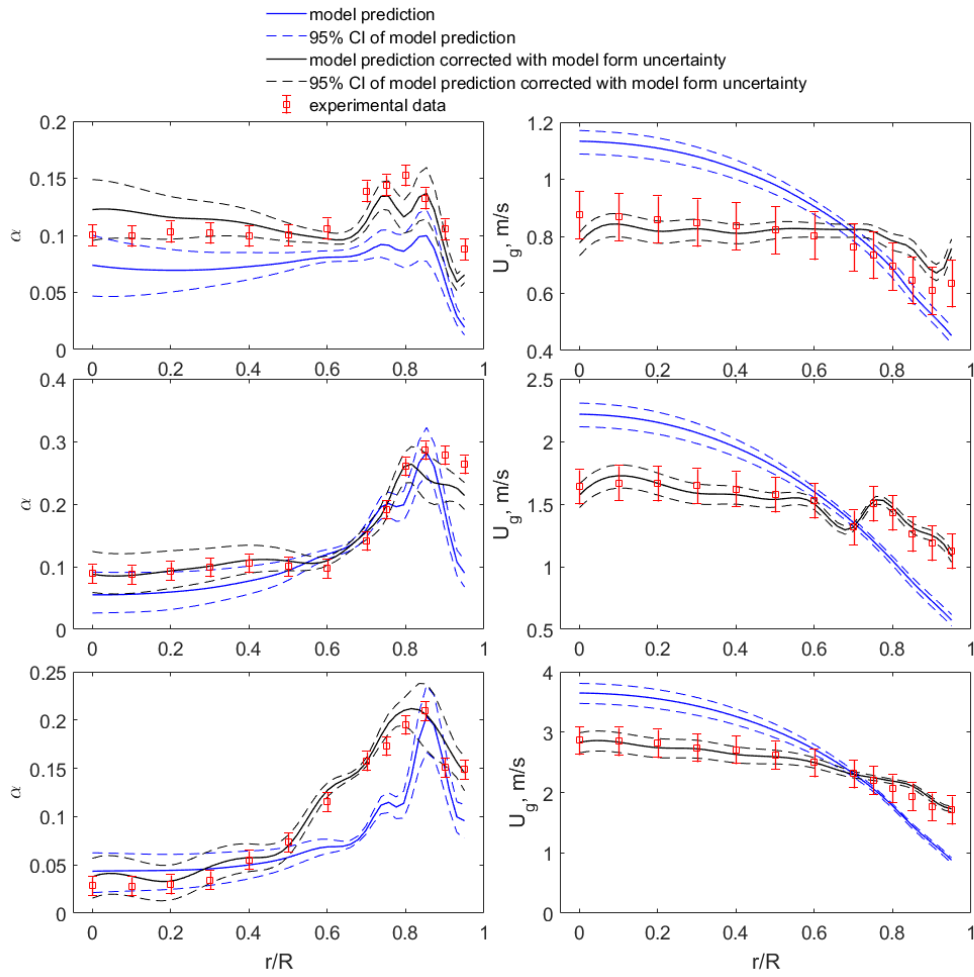


Figure 20. 95% confidence intervals of QoIs for model parameter uncertainty evaluation cases (first row: $j_g = 0.09$ m/s, $j_l = 0.64$ m/s; second row: $j_g = 0.29$ m/s, $j_l = 1.1$ m/s; third row: $j_g = 0.29$ m/s, $j_l = 2.0$ m/s)

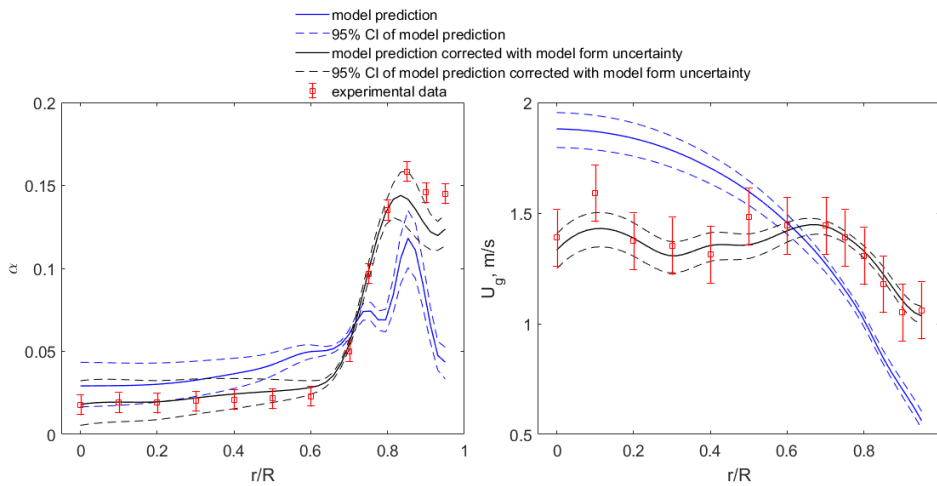


Figure 21. 95% confidence intervals of QoIs for test case ($j_g = 0.09$ m/s, $j_l = 1.1$ m/s)

It can be found from these three figures, the calibrated interfacial force closure relations can capture the near wall void fraction peak for all the conditions. The peak location can also be identified with acceptable accuracy. On the other hand, there are still relative large discrepancies between experimental data and solver prediction for the absolute values of void fraction. For the gas velocity, the solver predictions indicate a consistent pattern for all cases: underestimating the velocity in the near wall region while overestimating it in the central region. Such discrepancies, including the void fraction and gas velocity, can be corrected by adding the model form uncertainty term to the solver predictions. This indicate that there are significant model form uncertainties if the constant interfacial coefficients are chosen since significant information regarding the bubble dynamics flow are neglected. Moreover, it also demonstrates that the modular Bayesian approach can incorporate such model form uncertainty.

3.5 Validation metrics

The confidence interval and the area metric are calculated in this step. Three representative results, model form uncertainty evaluation case, model parameter uncertainty evaluation case and test case, are plotted in Figure 22 and Figure 23.

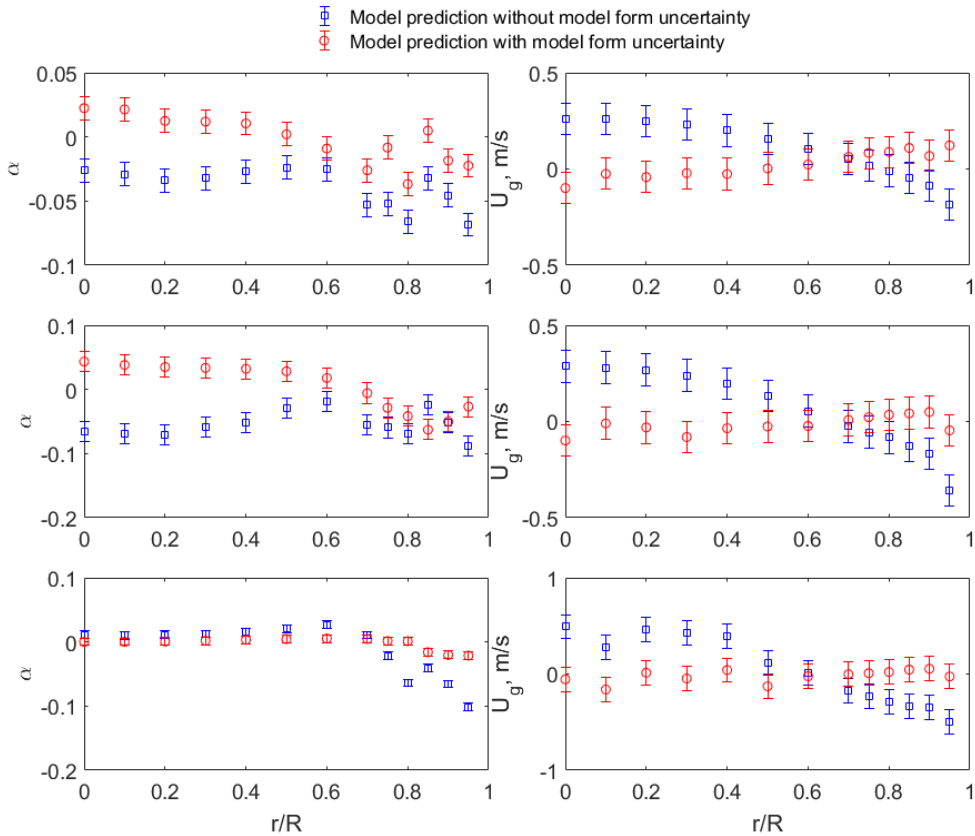


Figure 22. Confidence intervals for three representative cases (first row: $j_g = 0.09$ m/s, $j_l = 0.64$ m/s; second row: $j_g = 0.16$ m/s, $j_l = 0.64$ m/s; third row: $j_g = 0.09$ m/s, $j_l = 1.1$ m/s)

From the confidence interval plotted in Figure 22, several observations can be made:

- Generally, for void fraction, the model prediction is in better agreement with data in the central region than the near wall region. Such a pattern is most significant in the third case, $j_g = 0.09$ m/s, $j_l = 1.1$ m/s.

- For velocity, the confidence interval of error is positive in central region and negative in near wall region; this is consistent with the observation from uncertainty quantification results.
- With the consideration of model form uncertainty, the confidence interval of errors become very close to or covers zero. This reaffirmed that the model form uncertainty can be correctly accommodated with the modular Bayesian approach.

The area metrics of the same representative cases plotted in Figure 23 is consistent with the observations from confidence interval.

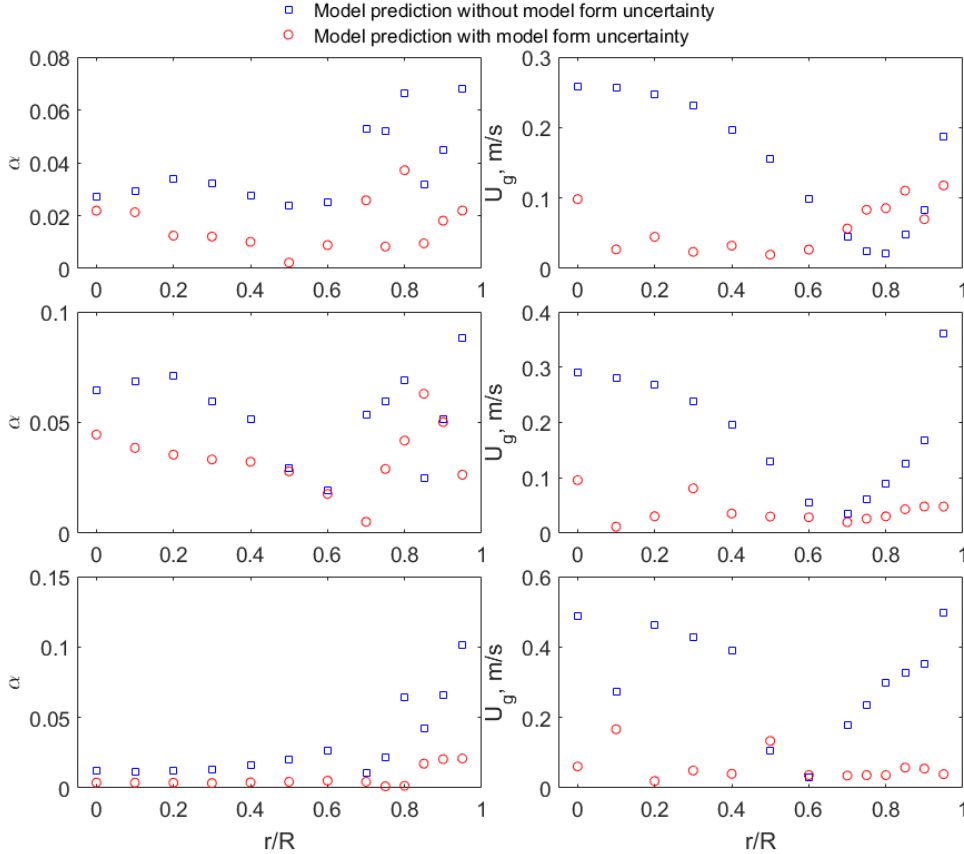


Figure 23. Area metrics for three representative cases (first row: $j_g = 0.09$ m/s, $j_l = 0.64$ m/s; second row: $j_g = 0.16$ m/s, $j_l = 0.64$ m/s; third row: $j_g = 0.09$ m/s, $j_l = 1.1$ m/s)

4. Conclusions

In this work, two case studies are performed to demonstrate the process of the VUQ framework designed for MCFD solver. One case study focuses on the wall heat transfer in the scenario of subcooled flow boiling in a vertical channel, whereas the other focuses on the flow dynamics in the scenario of adiabatic bubbly flow. Based on the VUQ results, several summaries can be drawn on the relevant closure relations of the MCFD solver:

- For both cases, only a subset of empirical parameters' uncertainties are quantified, whereas nominal values are employed to other parameters. There are two reasons for not quantifying the uncertainties of all parameters. Firstly, some parameters are not influential on the QoIs and thus do not need to be considered in the UQ process. Secondly, possible parameter identifiability issue could exist among certain parameters.

The UQ process will hence not update the prior distribution of these unidentifiable parameters. Given non-informative priors, this UQ process will lead to flat posteriors of these unidentifiable parameters, from which one can hardly get useful information for future simulation setup. In this sense, the parameter selection is an essential step for avoiding the parameter identifiability issue.

- For subcooled flow boiling case, the UQ results suggest that with the studied wall boiling closure relation, the MCFD solver can have predictions that are in good agreement with the wall superheat with experimental data, while having a relatively large model-data discrepancy on the wall heat transfer component. Such discrepancy can be quantified by the model form uncertainty term.
- For adiabatic bubbly flow, despite some discrepancy between solver prediction and experimental measurement, the void fraction predicted by MCFD solver, with calibrated interfacial force coefficients, can quantify the near wall peak observed in experimental measurement. But the predictions for bubble velocity tend to overestimate it in bulk flow region while underestimate it in near wall region. For both QoIs, the model-data discrepancy can be reduced by introducing the model form uncertainty term.

The obtained VUQ results confirm feasibility and basic promises of the proposed framework in several aspects:

- The surrogate modeling is found to be an effective method to alleviate the computation burden for performing the parametric study on MCFD solver.
- The uncertainties of closure relation parameters can be quantified through the inverse UQ with Bayesian inference. Since such UQ process is performed with datasets of different conditions instead of a single case study, the obtained results can be applied over the whole domain covered by data.
- There is significant model form uncertainty of the studied closure relations. These model form uncertainties can be evaluated through the modular Bayesian approach applied in the framework. On the other hand, this also emphasizes the importance to develop state-of-art closure relations that generalize more experimental evidence to reduce the model form uncertainty.
- The uncertainty of QoIs can be obtained by propagating the parameter uncertainties through the MCFD solver. Validation metrics are calculated to give a quantitative and objective measurement of the agreement between model predicted QoIs and the experimental measurement.

There are still several limitations of the current framework which requires improvement for further study:

- The numerical uncertainty is not explicitly evaluated in the framework. As a topic of verification, the numerical uncertainty is not discussed in this work. A more comprehensive evaluation requires the VUQ framework to be extended to the VVUQ.
- Whereas using the statistical model to construct a surrogate for the high dimensional output of the MCFD solver is helpful for significantly reducing the computation burden, additional uncertainties are introduced through this process. Such uncertainty is not evaluated in the current framework. The cross-validation can give an estimation of such

uncertainties by calculating the differences between original solver predictions and the predictions given by surrogate. However, whether such estimation can be extended to the whole validation domain is still unclear.

An additional topic that needs investigation is the data availability for the VUQ of MCFD solver. In current work, the VUQ on MCFD solver is decomposed into two separate case studies due to the limitation of experimental measurement. On the other hand, it should be noted that the high-fidelity simulation demonstrates its potential to be an alternative data source in addition to experiment. Moreover, the feasibility of using high-fidelity computational model to quantify the uncertainty of low-fidelity model has been demonstrated within statistical framework (Lewis et al., 2016). Based on this, the direct numerical simulations with interface tracking method for two phase flow and boiling (Feng and Bolotnov,2017), (Sato and Niceno,2017) could serve for the VUQ of MCFD solver.

Nomenclature

| | | |
|------------|--|---|
| a | effective bubble area factor | <i>Greek symbols</i> |
| A_b | effective bubble area fraction | α void fraction |
| C_d | drag coefficient | θ contact angle, rad |
| C_l | lift coefficient | σ surface tension, kg/s ² |
| C_{wl} | wall lubrication coefficient | σ^t turbulent dispersion coefficient |
| C_p | specific heat at constant pressure, J/(kg·K) | κ von Karman constant |
| C_{vm} | virtual mass coefficient | λ thermal conductivity, W/(m·K) |
| D_d | bubble departure diameter, m | μ_{con} contact angle scaler, rad |
| d_1 | departure diameter constant, m/rad | ρ density, kg/m ³ |
| e | bubble growth waiting time factor | |
| E | turbulence wall function Log law offset | <i>Subscripts</i> |
| f_d | bubble departure frequency, 1/s | g gas phase |
| g | gravity, m/s ² | sat saturated |
| h | specific enthalpy, J/kg | sup superheated |
| h_{fg} | latent heat of evaporation, J/kg | l liquid phase |
| h_l | forced convective heat transfer coefficient, W/(m ² ·K) | |
| N_a | nucleation site density, 1/m ² | |
| N_{avg} | averaged Nucleation site density coefficient, 1/m ² | |
| Pr^t | turbulent Prandtl number | |
| P | wall function coefficient | |
| q_{wall} | wall heat flux, W/m ² | |
| q_{Ev} | evaporation heat flux, W/m ² | |
| q_{Qu} | quenching heat flux, W/m ² | |
| q_{Fc} | forced convective heat flux, W/m ² | |

Acknowledgement

This research was partially supported by the Consortium for Advanced Simulation of Light Water Reactors (<http://www.casl.gov>), an Energy Innovation Hub (<http://www.energy.gov/hubs>) for Modeling and Simulation of Nuclear Reactors under U.S. Department of Energy Contract No. DE-AC05-00OR22725. and by Nuclear Energy University Program under the grant DE-NE0008530.

References

Antal S.P., Lahey R.T., Flaherty J.E., 1991. Analysis of phase distribution in fully developed laminar bubbly two-phase flow. *Int. J. Multiphase Flow*. 17(5), 635-652.

Auton T.R., Hunt J., Prud'Homme M., 1988. The force exerted on a body in inviscid unsteady non-uniform rotational flow. *J. Fluid Mech.* 197, 241-257.

Banks H.T., Cintron-Arias A., Kappel F., 2013. Parameter selection methods in inverse problem formulation. Book section in: *Mathematical modeling and validation in physiology*. Springer.

Bartolomei G.G. and Chanturiya V.M., 1967. Experimental study of true void fraction when boiling subcooled water in vertical tubes. *Thermal Engineering*. 14(2), 123-128.

Bucci M., Richenderfer A., Su G., McKrell T., Buongiorno J., 2016. A mechanistic IR calibration technique for boiling heat transfer investigations. *Int. J. Multiphase Flow*. 83, 115-127.

Cole R., 1967. Bubble frequencies and departure volumes at subatmospheric pressures. *AIChE J.* 13(4), 779-783.

Del Valle V.H. and Kenning D., 1985. Subcooled flow boiling at high heat flux. *Int. J. Heat Mass Transfer*. 28(10), 1907-1920.

Edeling W.N., Cinnella P., Dwight R.P., Bijl H., 2014. Bayesian estimates of parameter variability in the k-epsilon turbulence model. *Journal of Computational Physics*. 258, 73-94.

Feng J. and Bolotnov I.A., 2017. Effect of the wall presence on the bubble interfacial forces in a shear flow field. *Int. J. Multiphase Flow*. 99, 73-85.

Ferson S. and Oberkampf W.L., 2009. Validation of imprecise probability models. *International Journal of Reliability and Safety*. 3(1-3), 3-22.

Ferson S., Oberkampf W.L., Ginzburg L., 2008. Model validation and predictive capability for the thermal challenge problem. *Comput. Methods Appl. Mech. Eng.* 197(29), 2408-2430.

Gel A., Shahnam M., Musser J., Subramaniyan A.K., Dietiker J., 2016. Nonintrusive Uncertainty Quantification of Computational Fluid Dynamics Simulations of a Bench-Scale Fluidized-Bed Gasifier. *Ind Eng Chem Res.* 55(48), 12477-12490.

Gosman A.D., Lekakou C., Politis S., Issa R.I., Looney M.K., 1992. Multidimensional modeling of turbulent two-phase flows in stirred vessels. *AIChE J.* 38(12), 1946-1956.

Haario H., Laine M., Mira A., Saksman E., 2006. DRAM: efficient adaptive MCMC. *Stat Comput.* 16(4), 339-354.

Hibiki T. and Ishii M., 2003. Active nucleation site density in boiling systems. *Int. J. Heat Mass Transfer.* 46(14), 2587-2601.

Jayatilleke C., 1969. The influence of Prandtl number and surface roughness on the resistance of the laminar sublayer to momentum and heat transfer. *Prog. Heat Mass Transfer.* 1, 193-321.

Jung S. and Kim H., 2014. An experimental method to simultaneously measure the dynamics and heat transfer associated with a single bubble during nucleate boiling on a horizontal surface. *Int. J. Heat Mass Transfer.* 73, 365-375.

Kocamustafaogullari G., 1983. Pressure dependence of bubble departure diameter for water. *Int. Commun. Heat Mass Transfer.* 10(6), 501-509.

Krepper E., Končar B., Egorov Y., 2007. CFD modelling of subcooled boiling—concept, validation and application to fuel assembly design. *Nucl. Eng. Des.* 237(7), 716-731.

Kurul N. and Podowski M.Z., 1991. Multidimensional effects in forced convection subcooled boiling. in: *Proc. 9th International Heat Transfer Conference, Jerusalem, Israel.*

Leung W.H., Revankar S.T., Ishii Y., Ishii M., 1995. Axial development of interfacial area and void concentration profiles measured by double-sensor probe method. *Int. J. Heat Mass Transfer.* 38(3), 445-453.

Leung W.H., 1997. Modeling of interfacial area concentration and interfacial momentum transfer: Theoretical and experimental study (PhD Thesis). Purdue University, West Lafayette, IN.

Lewis A., Smith R., Williams B., Figueroa V., 2016. An information theoretic approach to use high-fidelity codes to calibrate low-fidelity codes. *J Comput Phys.* 324, 24-43.

Lin C. and Hibiki T., 2014. Databases of interfacial area concentration in gas–liquid two-phase flow. *Prog. Nuclear Energy.* 74, 91-102.

Liu T.J. and Bankoff S.G., 1993. Structure of air-water bubbly flow in a vertical pipe—II. Void fraction, bubble velocity and bubble size distribution. *Int. J. Heat Mass Transfer.* 36(4), 1061-1072.

Liu Y. and Dinh N., 2016. Analysis of heat transfer under high heat flux nucleate boiling conditions. *Kerntechnik*. 81(3), 308-314.

Marelli S. and Sudret B., 2014. UQLab: A framework for uncertainty quantification in Matlab. in: *Proc.2nd International Conference on Vulnerability and Risk Analysis and Management*, Liverpool, United Kingdom.

Oberkampf W.L. and Barone M.F., 2006. Measures of agreement between computation and experiment: validation metrics. *Journal of Computational Physics*. 217(1), 5-36.

Podowski R.M., Drew D.A., Lahey Jr R.T., Podowski M.Z., 1997. A mechanistic model of the ebullition cycle in forced convection subcooled boiling. in: *Proc.8th international topical meeting on nuclear reactor thermal-hydraulics*, Kyoto, Japan.

Pointer W.D. and Liu Y., 2017. Eulerian Two-Fluid RANS-based CFD Simulations of a Helical Coil Steam Generator Boiling Tube. in: *Proc.17th International Topical Meeting on Nuclear Reactor Thermal Hydraulics*, Xi'an China.

Richenderfer A. et al., 2017. The Application of Modern Experimental Techniques to The Study of Subcooled Nucleate Flow Boiling Including Critical Heat Flux. in: *Proc.17th International Topical Meeting on Nuclear Reactor Thermal Hydraulics*, Xi'an China.

Sato Y. and Niceno B., 2017. Nucleate pool boiling simulations using the interface tracking method: Boiling regime from discrete bubble to vapor mushroom region. *Int. J. Heat Mass Transfer*. 105, 505-524.

Weller H.G., Tabor G., Jasak H., Fureby C., 1998. A tensorial approach to computational continuum mechanics using object-oriented techniques. *Comput. Phys*. 12(6), 620-631.

Yoo J., Estrada-Perez C.E., Hassan Y.A., 2016. Experimental study on bubble dynamics and wall heat transfer arising from a single nucleation site at subcooled flow boiling conditions—Part 1: Experimental methods and data quality verification. *Int. J. Multiphase Flow*. 84, 315-324.